We are IntechOpen,
the world's leading publisher of
Open Access books
Built by scientists, for scientists

6,900
Open access books available

186,000
International authors and editors

200M
Downloads

154
Countries delivered to

Our authors are among the

TOP 1%
most cited scientists

12.2%
Contributors from top 500 universities

CLARIVATE ANALYTICS
BOOK CITATION INDEX
INDEXED

WEB OF SCIENCE™

Selection of our books indexed in the Book Citation Index
in Web of Science™ Core Collection (BKCI)

Interested in publishing with us?
Contact book.department@intechopen.com

Transperineal Targeted Biopsy with Real-Time Fusion Image of Multiparametric Magnetic Resonance Image and Transrectal Ultrasound Image for the Diagnosis of Prostate Cancer

Sunao Shoji

Additional information is available at the end of the chapter

Abstract

Objectives: To report clinical results of early experience of manually controlled targeted biopsy with real-time multiparametric magnetic resonance image (mpMRI)-transrectal ultrasound (TRUS) fusion images for the diagnosis of prostate cancer.

Methods: One hundred sixty-eight patients who were suspected of prostate cancer from mpMRI scans were recruited prospectively. We performed targeted biopsies for each cancer-suspicious lesion and 12 systematic biopsies using the BioJet® system. Pathological findings of targeted and systematic biopsies were analyzed.

Results: Median age of the 168 patients was 67 years (range: 52–89). Median preoperative prostate specific antigen (PSA) value was 6.9 ng/ml (range: 3.54–20). Median preoperative prostate volume was 37 ml (range: 22–68). The number of the cancer-detected cases was 99 (59%). The median biopsy time, included the MRI-TRUS fusion time and needle-punctured time without the anesthesia, was 8 minutes (range: 5–65). Cancer-detected rates of the systematic and targeted biopsy cores were 5.9 and 38%, respectively ($p < 0.0001$). In 25 patients who underwent radical prostatectomy, the geographic locations and pathological grades of clinically significant cancers and index lesions corresponded to the pathological results of the targeted biopsies.

Conclusion: The cancer cores detected by targeted biopsies with manually controlled targeted biopsy with real-time mpMRI-TRUS fusion image had significantly higher grades and larger length compared with those detected by the systematic biopsies. The further study of the comparisons with pathological findings of whole-gland specimens will give a larger role to the present biopsy method.

Keywords: prostate cancer, targeted biopsy, magnetic resonance image, transrectal ultrasound, fusion image

1. Introduction

Multiparametric magnetic resonance imaging (mpMRI) improves the imaging of prostate cancer lesion [1, 2], and several methods use MRI to guide the biopsy needle to target the cancer lesion. MRI-TRUS fusion image-guided biopsy achieved accurate prostate biopsy based on MRI, combining the superior sensitivity of MRI for targeting suspicious lesions with the practicality and familiarity of TRUS. MRI-TRUS fusion methods are used as visual registration [1, 3, 4] and fusion biopsy devices [5–9]. In visual registration, the TRUS operator identified the geographic location of the lesions in the prostate on the MRI, and then identify and biopsy viewing real-time TRUS [10]. In previous reports, the visual registration biopsy method improved accuracy over systematic biopsy [11–14]. However, the disadvantages of visual registration lie in human error when the targeted lesion was less than 10 mm in diameter [15]. Therefore, the visual registration is regarded as the prostate biopsy method for experts [10–14]. With the MRI-TRUS fusion devices, the stored MRI and real-time TRUS are superimposed using computer software to enable targeted biopsy of cancer-suspicious lesions [16]. MRI-TRUS fusion biopsy device "BioJet®" was approved by FDA after the evaluation of the accuracy with phantoms. We report the BioJet® experience of the manually controlled targeted biopsy using real-time fusion image from mpMRI and TRUS.

2. Methods

2.1. Population

From November 2013 to October 2015, after receiving the approval of institutional review board, the patients with PSA level greater than 4.0 ng/ml and less than 20 ng/ml were performed mpMRI prospectively. No patients had any previous history of prostate biopsy.

2.2. Multiparametric MRI

The MRI examination was carried out using a 1.5-Tesla magnet (Signa HDx®; GE Healthcare, Amersham Place, UK) with an 8-channel cardiac coil. T1-weighted fat-saturated axial fast spin-echo images (TR, 450 ms; TE, 8.8 ms; slice thickness, 3 mm; resolution, 0.9 × 1.3 mm) were obtained before injection. An intravenous bolus of 0.2 ml/kg of meglumine gadopentetate (Magnevist Syringe®; Bayer HealthCare Pharmaceuticals, Berlin, Germany) was then injected. All MRI examinations were performed using the same protocol, and included non-enhanced T2-weighted images (T2WI) (TR, 5000 ms; TE, 125 ms; slice thickness, 3 mm; resolution, 0.6 × 0.9 mm) acquired in the axial and sagittal planes, diffusion weighted image (DWI) and apparent diffusion coefficient (ADC) maps (b-value = 1500 s/mm^2), and dynamic-contrast-enhanced (DCE) MRI (resolution, 0.9 × 1.3 mm) using a fat-saturated T1-weighted fast-field echo sequence in the axial plane.

2.3. Image analysis

All mpMRI images, including T2WI, dynamic, DWI, and ADC map, were reviewed by two experienced radiologists with no prior clinical information. Suspicious areas, the so-called "regions of interest (ROI)", were provided a likelihood score that clinically significant cancer would be present for each ROI from 2 to 5 on the prostate imaging reporting and data system (PI-RAS) classification [17] based on Likert scale according to the European Society of Uro-genital Radiology Prostate MR Guidelines 2012 [18]: 1, most probably benign; 2, probably benign; 3, intermediate; 4, probably malignant; and 5, highly suspicious of malignancy [17] The location of each area was determined based on dividing the prostate into 27 regions, as described by Dickson et al. [16]. MRIs were imported into the biopsy fusion system. Segmentation into a two-dimensional (2D) mpMRI was performed on the workstation to create a 3D model of the MRI, and then fused to the real-time TRUS.

2.4. Biopsy protocol

A cleaning enema and antibiotics were given before the biopsy. TRUS with power Doppler was performed using a Prosound α7 (Hitachi Aloka Medical, Tokyo, Japan) equipped with a UST-678 transrectum composite probe, in the lithotomy position under spinal anesthesia. On the workstation, the operator fused the real-time TRUS image and 3D MRI model that included the prostate contour and ROI. After the elastic image fusion, an ultrasound probe was fixed to the arm that senses the 3D movement of the probe and exports the information to the workstation (**Figure 1a**). Using this device, the 2D image created from the 3D MRI model moves together with the real-time TRUS image on the workstation. The operator performed the biopsy using MRI-TRUS fusion image navigation (**Figure 1b**). During the procedure, the real-time ultrasound image is continuously available. The biopsy started with targeted biopsies to the center of cancer-suspicious lesions, and then 12 systematic biopsies were performed with transperineal technique in all patients. The biopsy used a standard brachytherapy grid with 5-mm spacing, with *x*-axis coordinates A through G and *y*-axis coordinates from 1 through 7, using D as the middle line urethral plane. An 18-gauge automatic biopsy gun with a specimen size of 22 mm (BARD® MAGNUM®, BARD MEDICAL, Covington, USA) was used to take biopsy cores. Using the interactive needle guide system, the biopsy template coordinates were shown on the monitor when the operator marked the target point of the ROI on the workstation (**Figure 2a, b**). The operator inserted the needle at the template coordinates and could get the prostate specimens by viewing the sagittal image of the prostate (**Figure 2c**). Immediately after each biopsy, the spatial punctured needle orbits were recorded in 2D TRUS image of axial and sagittal plane, and in the 3D model of MRI.

2.5. Pathological analysis

All biopsies were examined by expert pathologists. A significant cancer was defined as follows: at least one core with a Gleason score of 3 + 4 or 6 with a maximum cancer core length larger than 4 mm [19]. The pathological biopsy results were compared between systematic and targeted biopsies. The biopsy-proven index lesion of each patient was defined primarily as the lesion with the highest Gleason score, and secondarily as the lesion with the greatest cancer-

involved core in terms of length or percentage. Geographic location of prostate cancer in the prostate [16] was compared with pathologic step-sectioned prostatectomy specimens in the patients who were performed with radical prostatectomy.
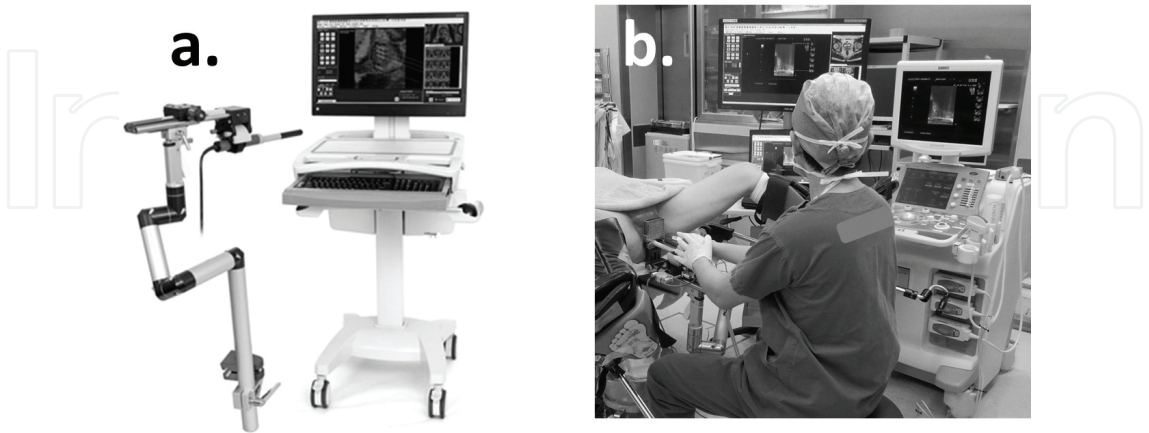

Figure 1. (a) BioJet system (D&K Technologies GmbH, Barum, Germany); (b) the set-up of prostate biopsy with BioJet system.
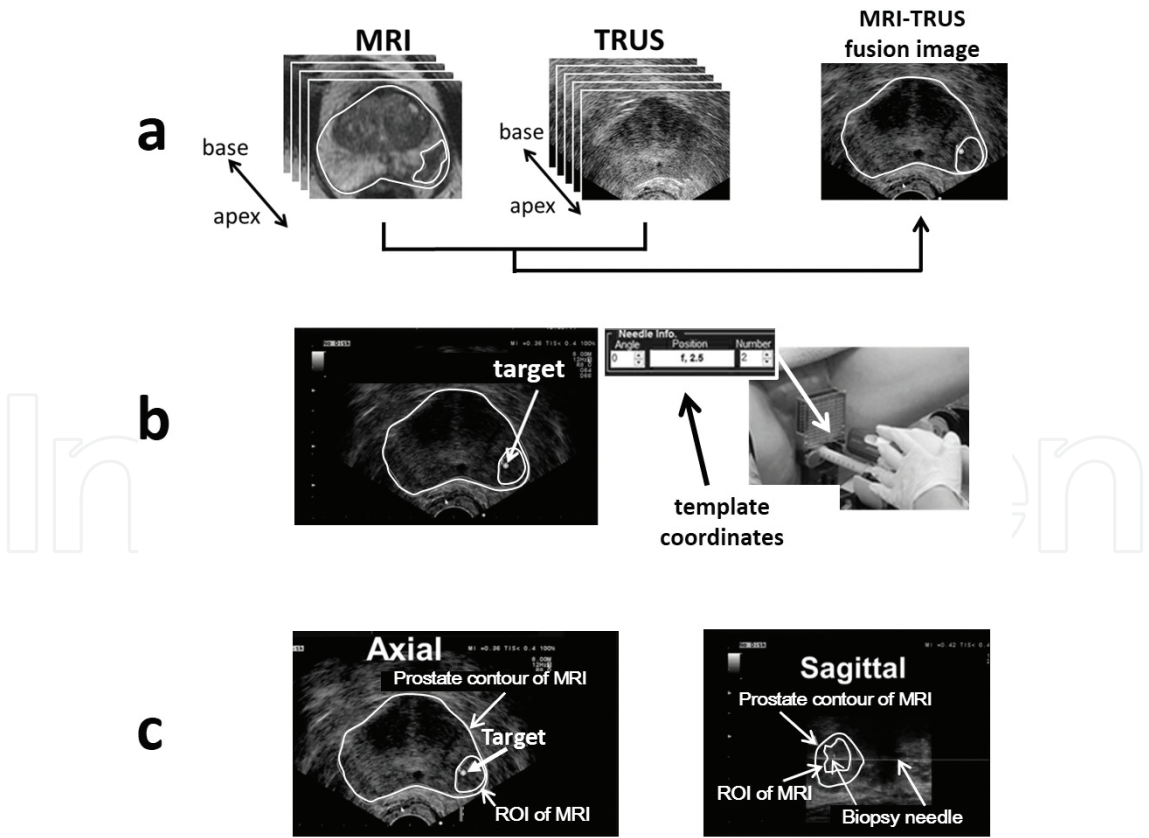

Figure 2. Process of prostate biopsy with BioJet system. (a) Fusion image from MRI and TRUS image. (b) Interactive needle guide system. (c) Real-time fusion images of axial and sagittal image.

2.6. Statistical analysis

All statistical analyses were performed using IBM SPSS® Statistics version 19 (IBM, Armonk, NY, USA). Among systematic and targeted biopsies, cancer-detected rate of biopsy, positive core length, positive core percentage, primary and secondary Gleason grade, and Gleason score were analyzed using the Mann-Whitney U-test. Changes in patient functional data were analyzed using paired *t*-tests. *P*-values of <0.05 were considered to indicate statistically significant differences.

3. Results

One-hundred sixty eight patients were suspected of prostate cancer with 2 to 5 of PI-RAD classification. The median age of the 168 patients was 67 years (range: 52–89). The median preoperative PSA value was 6.9 ng/ml (range: 3.54–20). The median preoperative prostate volume was 37 ml (range: 22–68). In the resected prostate specimen of 25 patients, the geographic locations and pathological grades of clinically significant cancers and index lesions corresponded to the results of the targeted biopsies.

The results of the prostate biopsies are shown in **Table 1**. The number of the cancer-detected cases was 99 (59%). The median biopsy time included the MRI-TRUS fusion time and needle-punctured time without the anesthesia, which was 8 minutes (range: 5–65). For the systematic and targeted biopsy cores, the total number of cores were 2016 and 372, respectively; the cancer-detected rates, the median positive core lengths, the median positive core percents, the median primary Gleason grades, the median secondary Gleason grades, and the median Gleason scores in systematic and targeted biopsy cores were significantly different.

	Target biopsy	Systematic biopsy	*P*-value
No. of biopsy cores	372	2016	n.d.
Rates of cancer detection	38%	5.9%	$p < 0.0001$
Rates of significant cancer detection	35%	1.4%	$p < 0.0001$
Median positive core lengths	8 mm (range: 1–22)	2 mm (range: 1–8)	$p < 0.0001$
Median positive core percents	60% (range: 5–100)	12% (range: 5–40)	$p < 0.0001$
Median primary Gleason grades	3 (3–5)	3 (3–4)	$p < 0.0001$
Median secondary Gleason grades	3 (3–5)	3 (3–4)	$p = 0.0020$
Median Gleason scores	6.5 (6–9)	6 (6–7)	$p = 0.0012$

Table 1. Biopsy results.

In targeted lesions of transition zone (TZ) (*n* = 146) and peripheral zone (PZ) (*n* = 226), the rate of cancer detection was 28% (*n* = 40) and 45% (*n* = 101), respectively. The rates of cancer detection and the corresponding scores on the PI-RAD in TZ and PZ are shown in **Table 2**.

	No. of target	PI-RADS classification	Rates of cancer detection		Rates of significant cancer detection	
TZ + PZ	372	2 (n = 70)	38% (n = 141)	4.3% (n = 3)	0% (n = 0)	
		3 (n = 126)		13% (n = 16)	10% (n = 13)	
		4 (n = 110)		61% (n = 67)	58% (n = 64)	
		5 (n = 71)		77% (n = 55)	77% (n = 55)	
TZ	146	2 (n = 28)	28% (n = 40)	7.1% (n = 2)	0% (n = 0)	
		3 (n = 40)		15% (n = 6)	10% (n = 4)	
		4 (n = 48)		24% (n = 12)	21% (n = 10)	
		5 (n = 35)		56% (n = 20)	56% (n = 20)	
PZ	226	2 (n = 42)	45% (n = 101)	2.4% (n = 1)	0% (n = 0)	
		3 (n = 86)		12% (n = 10)	11% (n = 9)	
		4 (n = 62)		88% (n = 55)	87% (n = 54)	
		5 (n = 36)		97% (n = 35)	97% (n = 35)	

TZ, transition zone; PZ, peripheral zone; PI-RADS, prostate imaging and reporting data system.

Table 2. The rates of cancer detection and the corresponding scores on the PI-RAD in transition zone and peripheral zone.

4. Discussion

Our results showed that cancer detection rates using targeted biopsies were significantly better than using systematic biopsies (p < 0.0001). Positive core length (p < 0.0001), positive core percent (p < 0.0001), primary (p < 0.0001) and secondary (p = 0.0020) Gleason grade, and Gleason score (p = 0.0012) were also significantly different between targeted and systematic biopsies. In addition, all biopsy-proven significant cancers were detected in ROIs, and the index lesions corresponded to the largest-sized ROIs. Based on these results, the targeted biopsy method was superior to systematic biopsy, and clinically significant cancers with a spatial relationship were detected accurately in the present study. Although the resected prostate specimens only comprised 25 cases, accuracy of the locations and pathological grades was reliable in our study.

In the present study, we used the T2WI for segmentation of the ROI, but the decision concerning the selection of ROI was made using multiparametric MRI factors, such as T2WI, DCE, DWI, and ADC maps because T2WI is sensitive but not specific for prostate cancer detection [1]. In mpMRI, the image values of its component techniques are different. T2WI provides the best depiction of the prostate's zonal anatomy and capsule in mpMRI and thus is used for prostate cancer detection and localization [18]. DCE is the most common imaging method for evaluating vascularity in the tumor [20]. DWI involves the quantification of free water motion [21] and allows ADC maps to be calculated, enabling qualitative and quantitative assessment of prostate cancer aggressiveness. Lower ADC corresponds to greater restriction in free water

motion, likely on the basis of increased cellularity compared with normal prostate tissue, and cancer shows a lower ADC value than normal prostate tissue [21]. Furthermore, ADC values correlate with Gleason scores [22–24]. However, some normal prostatic tissues, especially in the TZ, such as benign prostatic hyperplasia, chronic inflammation, and atrophic tissue, have similar findings of prostate cancer [16]. Indeed, the detection of prostate cancer in TZ was found difficulty in a previous study [23]. In our results, the cancer detection rate of the patients with a PI-RAD classification of 4 or 5 in TZ (39%) was inferior to that in PZ (92%).

The present device allows manually controlled targeted biopsy using real-time MRI-TRUS fusion images by the sensor arm of 3D movement. In addition, the fusion function has elastic fusion functions. The axial and sagittal view of US and MRI was useful to fuse the images of MRI and TRUS easily during the procedure. In addition, the present biopsy was performed with transperineal technique. Using the transperineal technique with the device, the biopsies were performed accurately to the ROIs. However, our study has limitations. First, our study did not compare biopsy results with pathological findings from whole-gland specimens. Therefore, although locations and pathological grades of clinically significant cancers and index lesions corresponded to the targeted biopsy results, it is difficult to exclude the possibility that a clinically important cancer has been missed without pathological analysis of whole-gland specimens.

In conclusion, cancers detected by targeted biopsies using manual controlled targeted biopsy with real-time fusion image of mpMRI and TRUS had a significantly higher grade and larger length compared with systematic biopsies. In present study, the cancer detection rate in TZ was significantly lower than in PZ. However, further study would contribute to set the cutoff point of PI-RADS scores in TZ and PZ to detect the prostate cancer at high frequency. The further study of the comparisons with pathological findings of whole-gland specimens will give a larger role to the present biopsy method.

Author details

Sunao Shoji

Address all correspondence to: sunashoj@mail.goo.ne.jp

Department of Urology, Tokai University Hachioji Hospital, Hachioji, Tokyo, Japan

References

[1] Moore CM, Kasivisvanathan V, Eggener S, et al. Standards of reporting for MRI-targeted biopsy studies (START) of the prostate: recommendations from an International Working Group. European Urology. 2013;64(4):544–552.

[2] Sciarra A, Barentsz J, Bjartell A, et al. Advances in magnetic resonance imaging: how they are changing the management of prostate cancer. European Urology. 2011;59(6): 962–977.

[3] Hambrock T, Somford DM, Hoeks C, et al. Magnetic resonance imaging guided prostate biopsy in men with repeat negative biopsies and increased prostate specific antigen. The Journal of Urology. 2010;183(2):520–527.

[4] Kasivisvanathan V, Dufour R, Moore CM, et al. Transperineal magnetic resonance image targeted prostate biopsy versus transperineal template prostate biopsy in the detection of clinically significant prostate cancer. The Journal of Urology. 2013;189(3): 860–866.

[5] Natarajan S, Marks LS, Margolis DJ, et al. Clinical application of a 3D ultrasound-guided prostate biopsy system. Urologic Oncology. 2011;29(3):334–342.

[6] Fiard G, Hohn N, Descotes JL, Rambeaud JJ, Troccaz J, Long JA. Targeted MRI-guided prostate biopsies for the detection of prostate cancer: initial clinical experience with real-time 3-dimensional transrectal ultrasound guidance and magnetic resonance/transrectal ultrasound image fusion. Urology. 2013;81(6):1372–1378.

[7] Mozer P, Roupret M, Le Cossec C, et al. First round of targeted biopsies with magnetic resonance imaging/ultrasound-fusion images compared to conventional ultrasound-guided trans-rectal biopsies for the diagnosis of localised prostate cancer. BJU International. 2014; 115(1): 50–57.

[8] Wysock JS, Rosenkrantz AB, Huang WC, et al. A prospective, blinded comparison of magnetic resonance (MR) imaging-ultrasound fusion and visual estimation in the performance of MR-targeted prostate biopsy: the PROFUS Trial. European Urology. 2014; 66(2):343:351.

[9] Marks L, Young S, Natarajan S. MRI-ultrasound fusion for guidance of targeted prostate biopsy. Current Opinion in Urology. 2013;23(1):43–50.

[10] Moore CM, Robertson NL, Arsanious N, et al. Image-guided prostate biopsy using magnetic resonance imaging-derived targets: a systematic review. European Urology. 2013;63(1):125–140.

[11] Haffner J, Lemaitre L, Puech P, et al. Role of magnetic resonance imaging before initial biopsy: comparison of magnetic resonance imaging-targeted and systematic biopsy for significant prostate cancer detection. BJU International. 2011;108(8 Pt 2):E171–E178.

[12] Park BK, Park JW, Park SY, et al. Prospective evaluation of 3-T MRI performed before initial transrectal ultrasound-guided prostate biopsy in patients with high prostate-specific antigen and no previous biopsy. AJR American Journal of Roentgenology. 2011;197(5):W876–W881.

[13] Sciarra A, Panebianco V, Ciccariello M, et al. Value of magnetic resonance spectroscopy imaging and dynamic contrast-enhanced imaging for detecting prostate cancer foci in

men with prior negative biopsy. Clinical Cancer Research: An Official Journal of the American Association for Cancer Research. 2010;16(6):1875–1883.

[14] Labanaris AP, Engelhard K, Zugor V, Nutzel R, Kuhn R. Prostate cancer detection using an extended prostate biopsy schema in combination with additional targeted cores from suspicious images in conventional and functional endorectal magnetic resonance imaging of the prostate. Prostate Cancer and Prostatic Diseases. 2010;13(1):65–70.

[15] Sonn GA, Margolis DJ, Marks LS. Target detection: magnetic resonance imaging-ultrasound fusion-guided prostate biopsy. Urologic Oncology. 2014;32(6):903–911.

[16] Dickinson L, Ahmed HU, Allen C, et al. Magnetic resonance imaging for the detection, localisation, and characterisation of prostate cancer: recommendations from a European consensus meeting. European Urology. 2011;59(4):477–494.

[17] Rothke M, Blondin D, Schlemmer HP, Franiel T. PI-RADS classification: structured reporting for MRI of the prostate. RoFo: Fortschritte auf dem Gebiete der Rontgenstrahlen und der Nuklearmedizin. 2013;185(3):253–261.

[18] Barentsz JO, Richenberg J, Clements R, et al. ESUR prostate MR guidelines 2012. European Radiology. 2012;22(4):746–757.

[19] Harnden P, Naylor B, Shelley MD, Clements H, Coles B, Mason MD. The clinical management of patients with a small volume of prostatic cancer on biopsy: what are the risks of progression? A systematic review and meta-analysis. Cancer. 2008;112(5): 971–981.

[20] Collins DJ, Padhani AR. Dynamic magnetic resonance imaging of tumor perfusion. Approaches and biomedical challenges. IEEE Engineering in Medicine and Biology Magazine: The Quarterly Magazine of the Engineering in Medicine & Biology Society. 2004;23(5):65–83.

[21] Gibbs P, Liney GP, Pickles MD, Zelhof B, Rodrigues G, Turnbull LW. Correlation of ADC and T2 measurements with cell density in prostate cancer at 3.0 Tesla. Investigative Radiology. 2009;44(9):572–576.

[22] Turkbey B, Shah VP, Pang Y, et al. Is apparent diffusion coefficient associated with clinical risk scores for prostate cancers that are visible on 3-T MR images? Radiology. 2011;258(2):488–495.

[23] Oto A, Kayhan A, Jiang Y, et al. Prostate cancer: differentiation of central gland cancer from benign prostatic hyperplasia by using diffusion-weighted and dynamic contrast-enhanced MR imaging. Radiology. 2010;257(3):715–723.

[24] Zelhof B, Pickles M, Liney G, et al. Correlation of diffusion-weighted magnetic resonance data with cellularity in prostate cancer. BJU International. 2009;103(7):883–888.